Applied Surface Science 366 (2016) 299–303

Contents lists available at ScienceDirect

Applied Surface Science

journal homepage: www.elsevier.com/locate/apsusc

Effect of profile and size of isolation trench on the optical and electrical performance of GaN-based high-voltage LEDs

Shengjun Zhou[a,b,*], Chenju Zheng[a], Jiajiang Lv[a], Yingce Liu[c], Shu Yuan[c], Sheng Liu[a], Han Ding[b]

[a] School of Power and Mechanical Engineering, Wuhan University, Wuhan 430072, China
[b] School of Mechanical Engineering, Shanghai Jiao Tong University, Shanghai 200240, China
[c] Quantum Wafer Inc., Foshan 528251, China

ARTICLE INFO

Article history:
Received 7 November 2015
Accepted 10 January 2016
Available online 12 January 2016

Keywords:
High voltage LEDs
Tapered GaN isolation trench
GaN etching
Light coupling propagation

ABSTRACT

Four types of HV-LEDs with different isolation trench width were presented. The isolation trench with an oblique angle of 45.6° was obtained using a combination of Cl_2/BCl_3 plasma chemistry and a thermally reflowed photoresist mask layer, enabling conformal metal lines coverage across the isolation trench. The effect of isolation trench width on the optical and electrical characteristics of HV LEDs was also investigated. A quantitative model was developed to analyze light coupling propagation phenomenon occurring within HV LEDs. The suppression of light coupling propagation among adjacent LED cells was achieved by extending isolation trench width from 3.81 μm to 12.30 μm, which improved light extraction efficiency and thus increased light output power of HV LEDs. However, the significantly increasing loss of MQW active region area, which was caused by further extending isolation trench width from 12.30 μm to 40.49 μm, decreased light output power of HV LEDs.

1. Introduction

Gallium nitride (GaN) is one of the most promising semiconductor materials that have been used for realization of blue/green/ultroviolet light-emitting diodes (LEDs) and laser diodes (LDs) [1–4]. The external quantum efficiency (EQE) of GaN-based LEDs reaches its peak at a low injection current density and then decreases with increasing injection current density, which is well known as efficiency droop [5–7]. To achieve higher light output power, the electrical power and the size of LED chip must be increased. However, high power LEDs with enlarged size suffers from poor current spreading performance [8–10]. To solve this problem, a large area LED chip can be divided into numerous serially connected LED cells, which is defined as high-voltage LEDs (HV-LEDs) [11–15]. Unlike high power LEDs driven by high current and low voltage, the HV-LEDs are driven by high voltage and low current, which opens up a new possibility of reducing efficiency droop. Moreover, the injection current can uniformly spread to the small and independent LED cells [16–18].

For HV-LEDs consisting of multiple serially connected LED cells, light rays emanating from multiple quantum well (MQW) travel through one LED cell might be absorbed by another adjacent LED cell, defined as light coupling propagation, result in a low light extraction efficiency. Yet there is now no analytical formulation and modeling to elucidate the light coupling propagation occurring within the HV-LEDs. To ensure LED cells within HV-LED chip are electrically isolated, deep isolation trenches terminating at the GaN/sapphire interface must be obtained by removing a portion of p-GaN layer, MQW active region and n-GaN layer [19,20]. This procedure leads to a reduction in effective area of MQW active region which is essential for LEDs to generate light, thus limiting light output power of HV-LEDs. However, the effect of reduced MQW active region area on the optical and electrical performance of HV-LEDs has not yet been investigated to date. In addition, the interconnection between LED cells is obtained through deposited metal lines. Since the deposited metal lines might not provide satisfactory step-coverage ability across the deep sharp-edged isolation trench which degrades reliability of interconnection between LED cells, tapered isolation trench with specific oblique angle is required to ensure reliable interconnection and improve yield of mass-produced HV-LEDs.

In this study, we presented the fabrication of deep isolation trench with an oblique angle of 45.6° and conformal metal lines coverage across the tapered isolation trench. By changing the width

* Corresponding author at: School of Power and Mechanical Engineering, Wuhan University, Wuhan 430072, China. Tel.: +86 158 2734 8861.
E-mail address: zhousj@whu.edu.cn (S. Zhou).

http://dx.doi.org/10.1016/j.apsusc.2016.01.068
0169-4332/

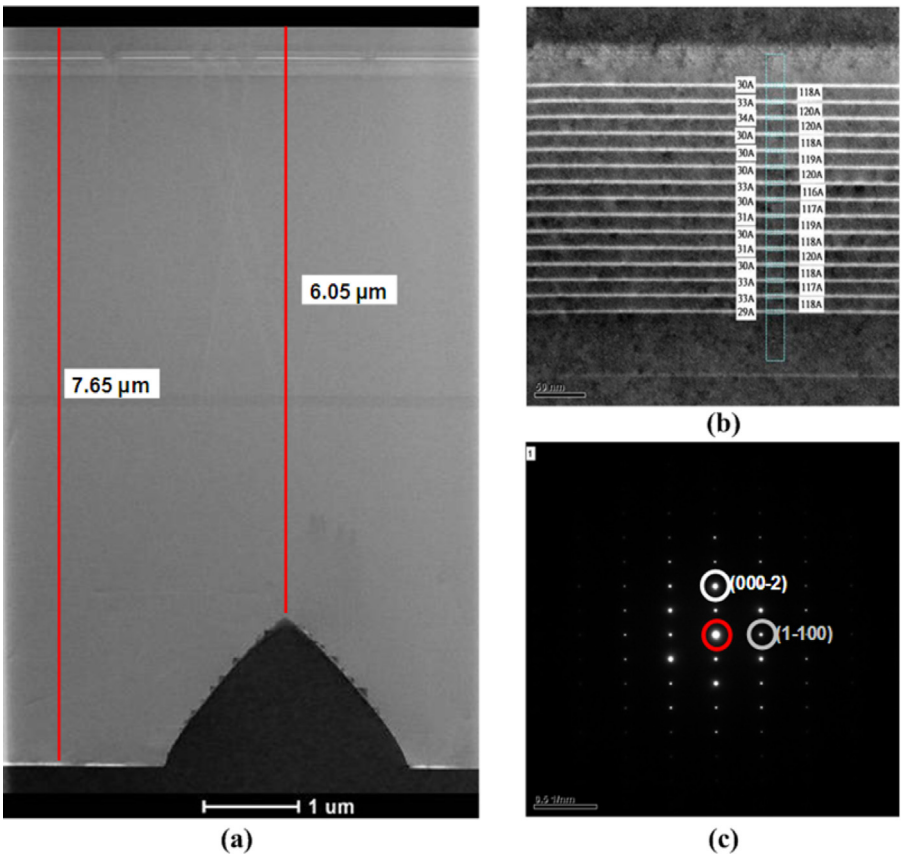

Fig. 1. (a) Cross-sectional TEM image of GaN grown on PSS. (b) High resolution TEM image of InGaN/GaN MQW grown on PSS. (c) SAD patterns of GaN.

of isolation trench, the effect of isolation trench width on the optical and electrical characteristics of HV-LEDs was also investigated in detail. An analytical formulation and modeling is developed to elucidate light coupling propagation phenomenon occurring in HV-LEDs.

2. Experiments

GaN-based LEDs were grown on the cone-shaped patterned sapphire substrate (PSS) by metal-organic chemical vapor deposition (MOCVD) equipment. Trimethylgallium (TMGa), trimethylindium

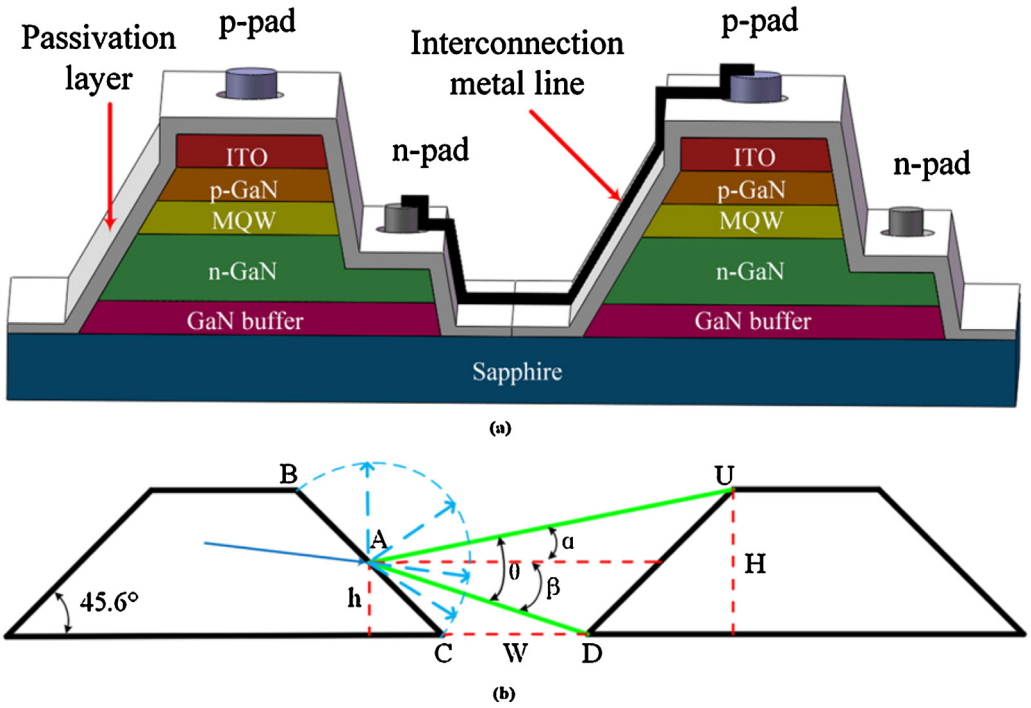

Fig. 2. (a) Schematic illustration of HV-LED layout. (b) Schematic illustration of light coupling propagation between adjacent LED cells.

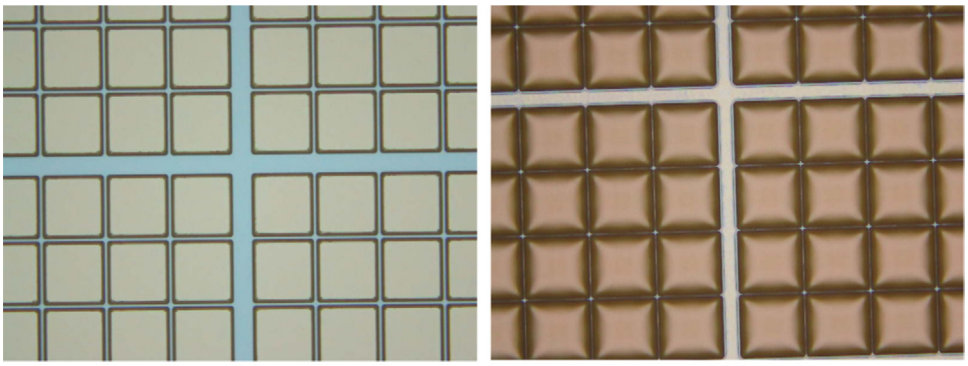

Fig. 3. (a) Optical microscopy image of coating photoresist before hard baking process. (b) Optical microscopy image of coating photoresist after hard baking process.

(TMIn), and ammonia (NH_3) were used as precursors. Silane (SiH_4) and biscyclopentadienylmagnesium (Cp_2Mg) were used as the n-dopant and p-dopant source, respectively. The LEDs consisted of a 30-nm-thick GaN nucleation layer, a 2.2-μm-thick undoped GaN buffer layer, a 2.5-μm-thick Si-doped n-GaN layer, a 400-nm-thick InGaN/GaN superlattice stress release layer, a InGaN/GaN multiple quantum well (MQW), a 110-nm-thick Mg doped p-AlGaN electron blocking layer, and a 5-nm-thick heavily Mg-doped p++-GaN. The InGaN/GaN MQW structure involved 12 pairs of 3-nm-thick $In_{0.16}Ga_{0.84}N$ well layers and 12-nm-thick GaN barrier layer. After GaN epitaxial growth process was completed, the activation of the Mg acceptors in the as-grown p-GaN layer is achieved by thermal annealing at 750 °C in N_2 atmosphere.

Inductively coupled plasma etching (ICP) process based on BCl_3/Cl_2 plasmas was used to etch the LED samples until the n-GaN layer was exposed with an etch depth of about 1.2 μm. The isolation trench with an etch depth of about 7.65 μm was obtained by combining photolithography and subsequent ICP deep etching process based on BCl_3/Cl_2 plasmas [21–23]. A 60-nm-thick SiO_2 passivation layer was deposited by using plasma-enhanced chemical vapor deposition (PECVD) method to prevent short circuits among LED cells. An indium tin oxide (ITO) transparent conductive layer was deposited on the top of p-GaN layer using electronic beam evaporator and was subsequently annealed at 540 °C for 10 min in N_2 atmosphere to improve ohmic contact between ITO and p-GaN; Cr/Pt/Au interconnect metal lines and p/n-electrodes were simultaneously evaporated onto LED samples using electronic beam evaporator. We fabricated and characterized four types of HVLEDs with different isolation trench width of 3.81 μm (HV-LED I), 6.38 μm (HV-LED II), 12.30 μm (HV-LED III) and 40.49 μm (HV-LED IV), respectively. The profile of etched isolation trench was observed using scanning electron microscopy (SEM, Zeiss Sigma). The optical and electrical characteristics of HVLEDs were measured using a probe station system [24].

3. Results and discussion

Fig. 1a illustrated the bright filed transmission electron microscopy (TEM) image of GaN grown on PSS. The total thickness of as-grown GaN epitaxial layer was approximately 7.65 μm, and the distance between the apex of PSS and the p-GaN was about 6.05 μm. Isolation among the LED cells requires complete removal of GaN epitaxial layer. Therefore, a total etch depth of 7.65 μm was required to form isolation trench. Fig. 1b showed TEM image of InGaN/GaN MQW grown on PSS. Fig. 1c demonstrated the selected-area diffraction (SAD) patterns of GaN. The incident electron beam azimuth was parallel to $[\bar{1}\,2\,\bar{1}\,0]$ GaN.

Fig. 2a showed the layout of monolithically integrated HV-LEDs. The LED cells were electrically isolated from each other by the deep

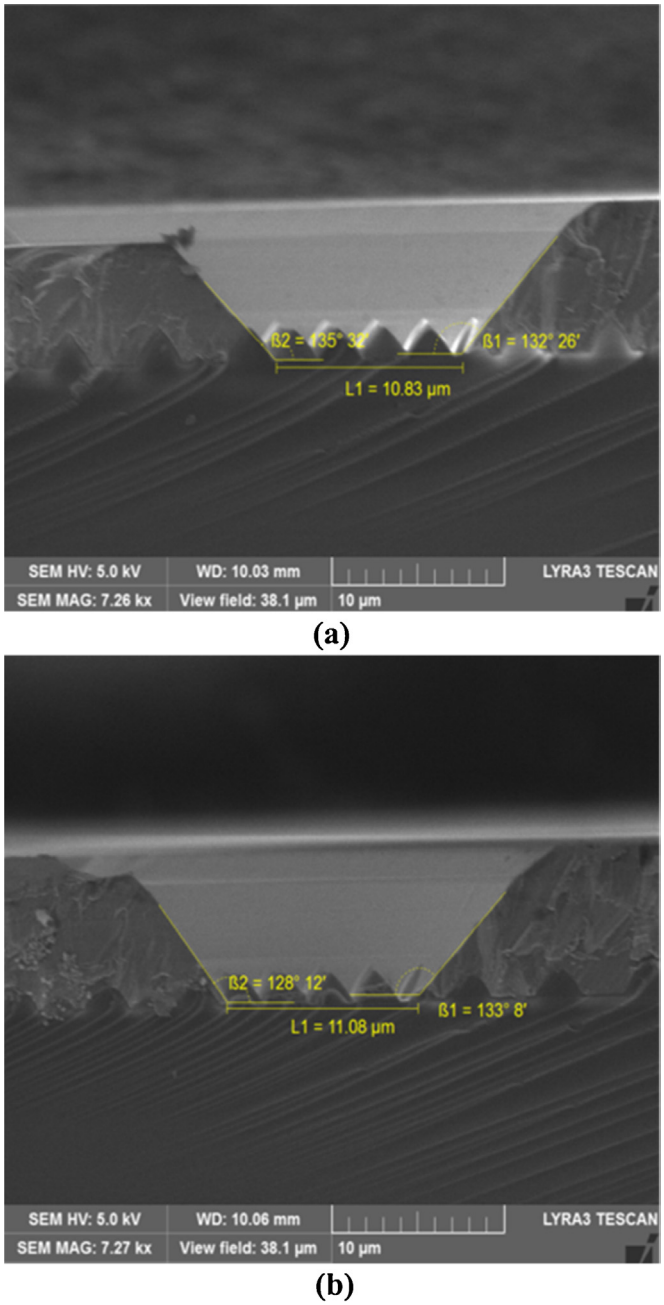

Fig. 4. (a) Profile of isolation trench with an etching time of 1800 s. (b) Profile of isolation trench with an etching time of 1950 s.

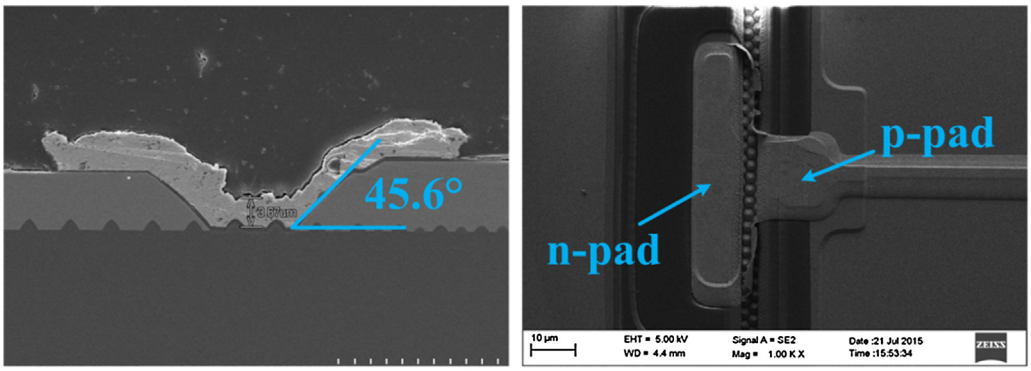

Fig. 5. (a) Cross-sectional SEM image of tapered isolation trench sidewall with an oblique angle of 45.6°. (b) Top-view SEM image of interconnected LED cells via Cr/Pt/Au metal lines.

isolation trench with oblique sidewall as shown in Fig. 2a. The sidewalls of isolation trench were covered with a SiO_2 insulation layer so as to prevent leakage current. Fig. 2b showed an analytical formulation and modeling, which was developed to elucidate the light coupling propagation occurring among the LED cells. In Fig. 2b, random point A is chosen along the sidewall of one of the LED cells, W denotes isolation trench width, H indicates the depth of the isolation trench and h shows the vertical distance from point A to the base. Light rays emanating from MQW travel through point A into the space in all directions (from AB to AC), but only those within green lines AU and AD can be absorbed by another adjacent LED cell. After simple mathematical derivation, equations that clarify the relation of the variants are given by

$$\tan\alpha = \frac{H-h}{H+h+W} \tag{1}$$

$$\tan\beta = \frac{h}{h+W} \tag{2}$$

$$\theta = \alpha + \beta \tag{3}$$

Light absorption ratio can be expressed as

$$\eta = \frac{\theta}{\pi} \tag{4}$$

From the equations above, we can conclude that for every single point A, light absorption ratio η declines while the isolation trench width (W) increases. In other words, when the isolation trench width is narrowed, more light rays emanating from one LED cell will be absorbed by adjacent LED cells due to stronger light coupling propagation, which results in lower light extraction efficiency. Although light coupling propagation among LED cells can be effectively suppressed by extending isolation trench width, the

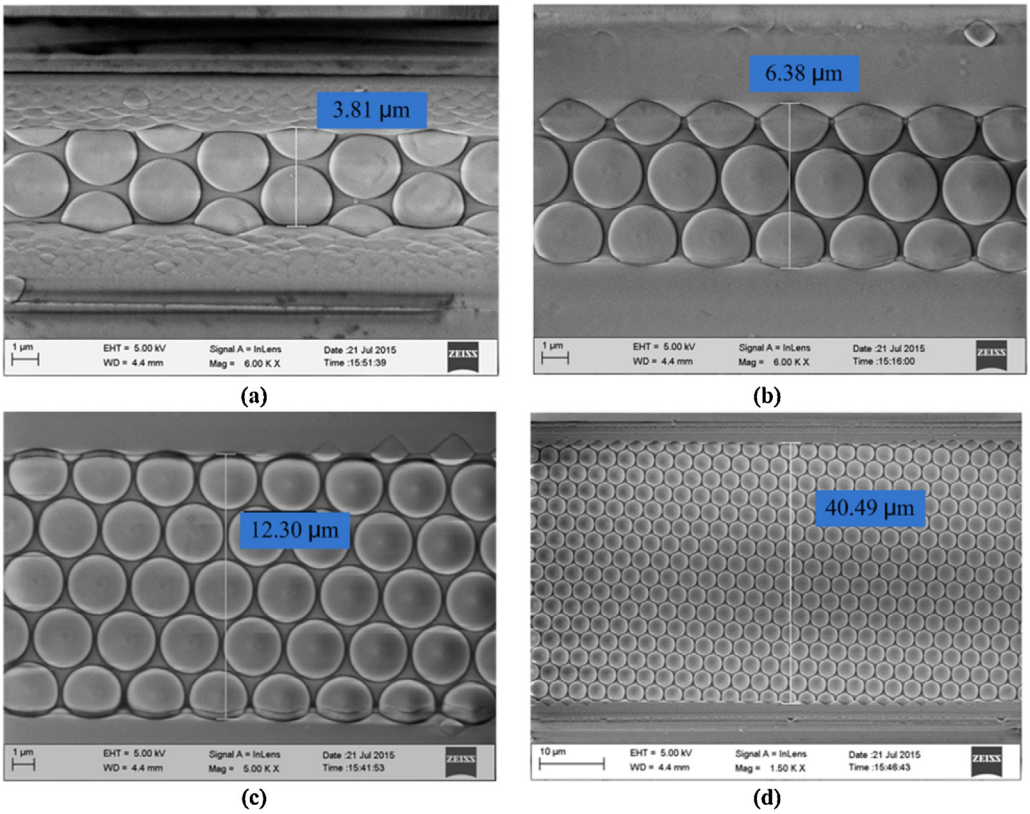

Fig. 6. (a) SEM image of etched isolation trench with a width of 3.81 μm. (b) SEM image of etched isolation trench with a width of 6.38 μm. (c) SEM image of etched isolation trench with a width of 12.30 μm. (d) SEM image of etched isolation trench with a width of 40.49 μm.

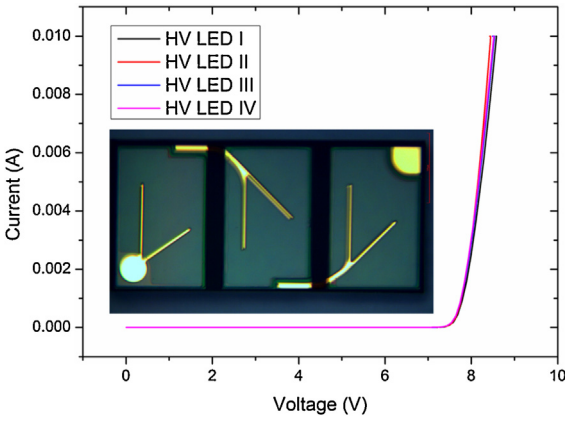

Fig. 7. *I–V* characteristics of HVLEDs with different isolation trench width. The inset is optical microscopy of fabricated HV-LEDs.

loss of MQW active region area would be enlarged, thereby reducing the ability of LED to generate light. Therefore, a tradeoff exists between light extraction efficiency and MQW active region area, creating a compromised HV-LEDs design that limits light output power.

Due to its physical hardness and chemical stability, etch rate of GaN is relatively low. Thick photoresist film is therefore required for GaN deep etching due to low etch selectivity. During the photolithography process, a positive tone EXP-1520T photoresist of 8-μm-thick was spin-coated onto LED wafer. Next, the EXP-1520T photoresist was patterned to be a rectangle shape (Fig. 3a) and then reflowed during a hard baking process on an oven chamber for 10 min at 120 °C to make resist profile tapered (Fig. 3b).

After tapered photoresist profile was obtained by thermally reflowed process, GaN epitaxial layer was then etched and tapered photoresist profile could be transfer into the etched isolation trench. During the deep etching process, the etch rate of GaN was 220 nm/min, and GaN etch selectivity over photoresist was 1.12 while maintaining 350 W ICP power/375 RF power, 115 sccm Cl_2/5 sccm BCl_3, and 5 mTorr operating pressure. The isolation trenches with different angles were obtained by changing the etching time as showed in Fig. 4.

Fig. 5a demonstrated the cross-sectional SEM image of etched isolation trench with deposited interconnection metal lines. A tapered isolation trench with an oblique angle of 45.6° was observed as shown in Fig. 5a, which enabled the Cr/Pt/Au metal line to overlay the trench smoothly. Fig. 5b showed top-view SEM image of interconnected LED cells. The n-pad of one LED cell was connected to the other adjacent LED cell via Cr/Pt/Au metal line as shown in Fig. 5b.

Fig. 6 showed top-view SEM image of etched isolation trench with different width. To clarify the effect of isolation trench width on the optical and electrical characteristics of HV-LEDs, the width of isolation trench was varied to be 3.81 μm (Fig. 6a), 6.38 μm (Fig. 6b), 12.30 μm (Fig. 6c) and 40.49 μm (Fig. 6d), respectively. After an etch depth of 7.65 μm was achieved, the PSS can be clearly observed as shown in Fig. 6, indicating complete removal of GaN epitaixial layer.

Fig. 7 showed *I–V* characteristics of fabricated HV-LEDs with isolation trench width of 3.81 μm (HV-LED I), 6.38 μm (HV-LED II), 12.30 μm (HV-LED III) and 40.49 μm (HV-LED IV). At 10 mA injection current, the forward voltages of HV-LED I, HV-LED II, HV-LED III and HV-LED IV were measured to be 8.57 V, 8.42 V, 8.49 V and 8.51 V, respectively. The almost consistent *I–V* characteristics indicated that there was no significant leakage current occurring in these HV-LEDs, thus testifying that complete isolation and reliable interconnection were obtained through isolation trench with tapered profile.

At an injection current of 10 mA, the light output powers of LED I (3.81 μm), LED II (6.38 μm), LED III (12.30 μm) and LED IV (40.49 μm) were measured to be 170 mW, 176 mW, 185 mW and 150 mW, respectively. An increase in light output power of HV-LEDs was observed as isolation trench width was increased from 3.81 μm (LED I) to 6.38 μm (LED II) and then to 12.30 μm (LED III). The improvement was ascribed to the effect of suppression in light coupling propagation among adjacent LED cells by extending isolation trench width, where the effect of the loss of MQW active region area were not so prominent as that of the suppression in light coupling propagation. However, the light output power of HV-LED IV with isolation trench width of 40.49 μm was 18.9% lower than that of HV-LED III with isolation trench width of 12.30 μm. This decrease was attributed to a markedly increasing loss of MQW active region area, which led to so significant decrease of light output power that surpassing the increase of light output power induced by suppression of light coupling propagation phenomenon.

4. Conclusions

In conclusion, we fabricated four types of HV-LEDs with different isolation trench width. The isolation trench with an oblique angle of 45.6° was obtained, enabling interconnection metal line to overlay the trench smoothly and thus improving yield of mass-produced HV-LEDs. An analytical formulation and modeling was developed to elucidate the light coupling propagation among adjacent LED cells. When the decrease of light output power caused by loss of MQW active region area surpassed the increase of light output power induced by suppression of light coupling phenomenon among LED cells, the light output power of HV-LEDs would start to decrease as the increasing isolation trench width.

Acknowledgments

This work was supported by the Project of the National Natural Science Foundation of China (No. 51305266) and the National High-tech R&D Program of China (863 Program Grant No. 2015AA03A101).

References

[1] M. Iwaya, S. Terao, N. Hayashi, T. Kashima, H. Amano, I. Akasaki, Appl. Surf. Sci. 159 (2000) 405.
[2] S. Nakamura, T. Mukai, M. Senoh, N. Iwasa, Jpn. J. Appl. Phys. 31 (1992) L139.
[3] X.L. Hu, L. Liu, H. Wang, X.C. Zhang, Appl. Surf. Sci. 357 (2015) 1703.
[4] S. Zhou, B. Cao, S. Yuan, S. Liu, Appl. Opt. 53 (2014) 8104.
[5] J. Iveland, L. Martinelli, J. Peretti, J.S. Speck, C. Weisbuch, Phys. Rev. Lett. 110 (2013) 177406.
[6] B. Cao, S. Li, R. Hu, S. Zhou, Y. Sun, Z. Gan, S. Liu, Opt. Express 21 (2013) 25381.
[7] E. Jung, G. Hwang, J. Chung, O. Kwon, J. Han, Y.T. Moon, T.Y. Seong, Appl. Phys. Lett. 101 (2012) 081120.
[8] S. Zhou, S. Yuan, Y. Liu, L.J. Guo, S. Liu, H. Ding, Appl. Surf. Sci. 355 (2015) 1013.
[9] H.Y. Ryu, J.I. Shim, Opt. Express 19 (2011) 2886.
[10] S. Zhou, S. Liu, H. Ding, Opt. Laser Technol. 47 (2013) 127.
[11] W. Wang, Y. Cai, Y.B. Zhang, H.J. Huang, W. Huang, H.O. Li, B.S. Zhang, Phys. Stat. Sol. RRL 8 (2014) 260.
[12] S.J. Chang, C.Y. Chang, C.L. Tseng, C.S. Shen, B.Y. Chen, IEEE Photonics Technol. Lett. 26 (2014) 1073.
[13] T.H.H. Yen, W.Y. Yeh, H.C. Kuo, Phys. Stat. Sol. (a) 204 (2007) 2077.
[14] T. Tamura, T. Setomoto, T. Taguchi, J. Lumin. 87 (2000) 1180.
[15] C. Tien, K. Chen, C. Hsu, R. Horng, Opt. Express 22 (2014) A1462.
[16] C.H. Wang, D.W. Lin, C.Y. Lee, M.A. Tsai, G.L. Chen, H.T. Kuo, W.H. Hsu, H.C. Kuo, T.C. Lu, S.C. Wang, G.C. Chi, IEEE Electron Device Lett. 32 (2011) 1098.
[17] R.H. Horng, K.C. Shen, Y.W. Kuo, D.S. Wuu, ECS Solid State Lett. 1 (2012) R21.
[18] S.G. Li, K.T. Lam, W.C. Huang, S.J. Chang, J. Photon Energy 5 (2015) 057605.
[19] S. Zhou, B. Cao, S. Liu, Appl. Phys. A 105 (2011) 369.
[20] G.Y. Mak, E.Y. Lam, H.W. Choi, J. Vac. Sci. Technol. B 29 (2011) 011025.
[21] D.S. Rawal, H. Arora, B.K. Sehgal, R. Muralidharan, J. Vac. Sci. Technol. A 32 (2014) 031301.
[22] S. Zhou, B. Cao, S. Liu, Appl. Surf. Sci. 257 (2010) 905.
[23] G.F. Yang, Y. Guo, H.X. Zhu, D.W. Yan, G.H. Li, S.M. Gao, K.X. Dong, Appl. Surf. Sci. 285 (2013) 772.
[24] S. Zhou, S. Liu, Rev. Sci. Instrum. 80 (2009) 095102.